Environmental Science & Technology

pubs.acs.org/est

Article

Tide-Triggered Production of Reactive Oxygen Species in Coastal Soils

Guoqiang Zhao, Binbin Wu, Xiaoshan Zheng, Baoliang Chen, Andreas Kappler, and Chiheng Chu*

Cite This: *Environ. Sci. Technol.* 2022, 56, 11888−11896

Read Online

ACCESS | Metrics & More | Article Recommendations | Supporting Information

ABSTRACT: We report an unrecognized, tidal source of reactive oxygen species (ROS). Using a newly developed ROS-trapping gel film, we observed hot spots for ROS generation within ∼2.5 mm of coastal surface soil. Kinetic analyses showed rapid production of hydroxyl radicals ($^{\bullet}OH$), superoxide ($O_2^{\bullet-}$), and hydrogen peroxide (H_2O_2) upon a shift from high tide to low tide. The ROS production exhibited a distinct rhythmic fluctuation. The oscillations of the redox potential and dissolved oxygen concentration followed the same pattern as the $^{\bullet}OH$ production, suggesting the alternating oxic−anoxic conditions as the main geochemical drive for ROS production. Nationwide coastal field investigations confirmed the widespread and sustainable production of ROS via tidal processes (22.1−117.4 μmol/m^2/day), which was 5- to 36-fold more efficient than those via classical photochemical routes (1.5−7.6 μmol/m^2/day). Analyses of soil physicochemical properties demonstrated that soil redox-metastable components such as redox-active iron minerals and organic matter played a key role in storing electrons at high tide and shuttling electrons to infiltrated oxygen at low tide for ROS production. Our work sheds light on a ubiquitous but previously overlooked tidal source of ROS, which may accelerate carbon and metal cycles as well as pollutant degradation in coastal soils.

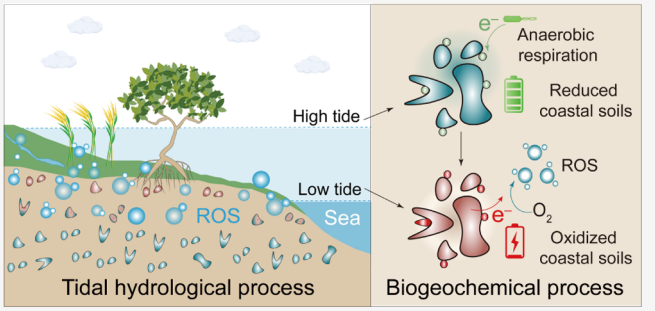

KEYWORDS: *reactive oxygen species (ROS), coast, tide, soil biogeochemistry, redox fluctuations*

INTRODUCTION

Reactive oxygen species (ROS) are ubiquitous on the earth's surface and profoundly influence element cycles[1,2] and pollutant dynamics.[3,4] Historically, the ROS productions on the earth's surface are suggested to be dominated by photochemical processes exerted by the sun,[5] leaving the role of ROS in soil biogeochemical processes overlooked due to limited sunlight penetration depth (<0.5 mm).[6,7] Recent studies reveal a dark production of ROS through exposure of extracellular electrons produced by anaerobic microbial respiration to oxygen during an intermittent redox turnover (e.g., seasonal mixing in stratified lakes).[8−10] Moreover, reduced geomaterials (e.g., Fe and S minerals and organic matter) can activate oxygen to produce ROS.[11−13] For instance, water table fluctuation in inland shallow aquifers regulated the redox conditions of geomaterials and produced ROS.[14] In natural systems, those small-scale biogeochemical processes could be triggered by large-scale hydrological fluctuations.[15] Yet, a link between biogeochemical and hydrological processes for ROS productions remains largely unestablished.

Coastal ecosystems such as intertidal mangroves and saltmarshes are widespread hot spots for biogeochemical−hydrological interactions[16] and play an outsized role as global carbon[17] and pollutants (e.g., crude oil,[18] pesticides, etc.).[19] The tidal fluctuations could induce frequent redox oscillations in coastal soils.[20,21] Such redox oscillations could lead to the contact of infiltrated oxygen and reduced substance that are abundant in coastal soils (e.g., ferrous minerals, sulfide, and organic matter), creating the prerequisite for ROS productions (Figure 1a).[5,22] Therefore, we were interested in whether tide-induced redox fluctuations indeed trigger ROS productions, which, if the case, will greatly impact element and pollutant redox cycles in coastal ecosystems.

The goal of this study was to investigate whether tide can fuel ROS productions in coastal soils. Specifically, we aim to (i) detect tide-triggered ROS production in coastal soils with a spatial and temporal resolution, (ii) explore the ROS production sustainability and rhythm under alternating tidal conditions, (iii) examine whether the tide-triggered ROS production was ubiquitous in natural systems with varying biogeochemical and climatic conditions, and (iv) reveal the role of soil electron-storing geobattery materials (e.g., Fe and S

Received: May 3, 2022
Revised: June 23, 2022
Accepted: June 28, 2022
Published: July 11, 2022

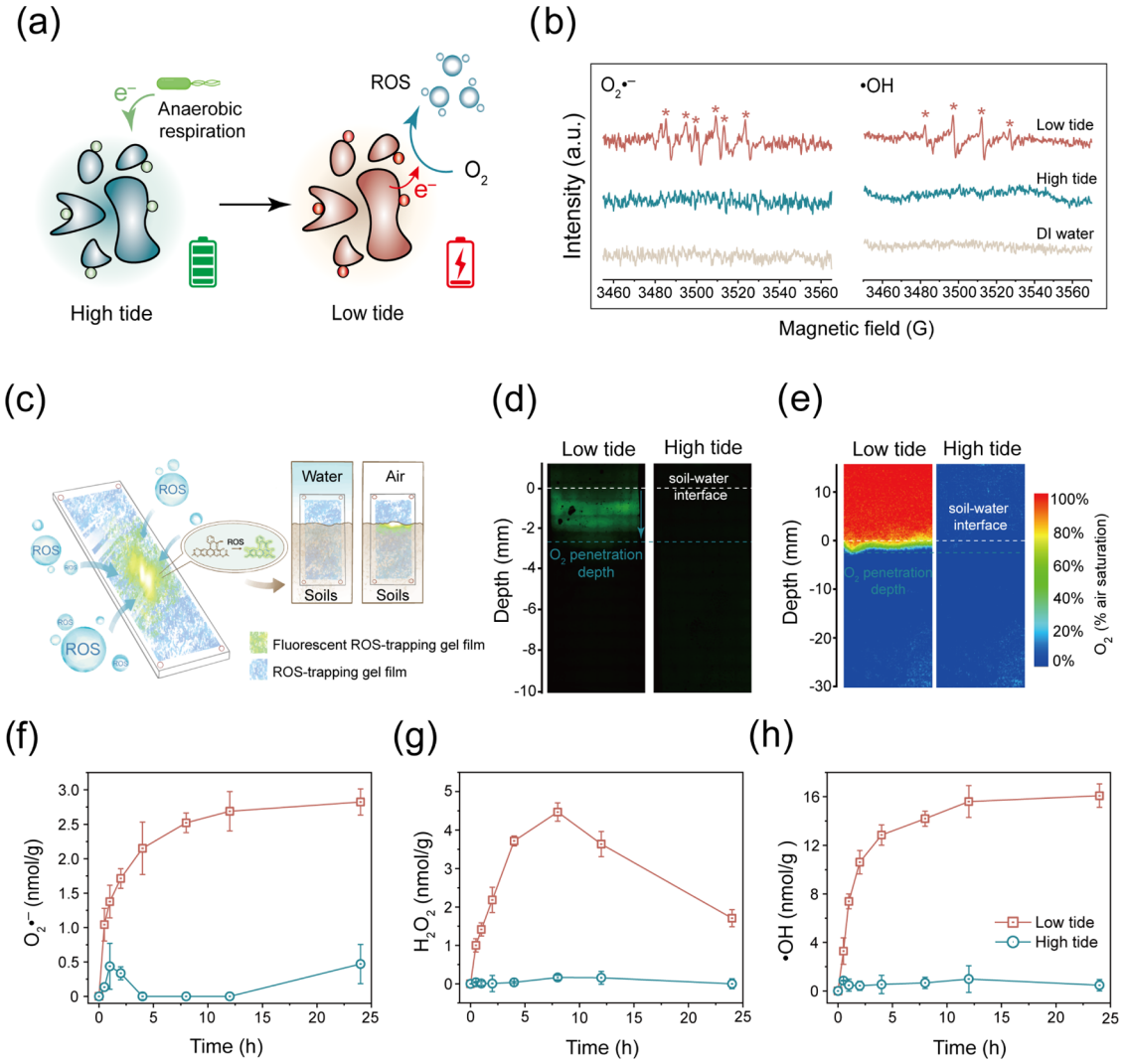

Figure 1. Tide-triggered ROS production in coastal soils. (a) Schematic illustration of ROS production in coastal soils upon a shift from high tide to low tide. The contact of infiltrated oxygen at low tide with reduced substances could lead to ROS production. (b) Production of $O_2^{\bullet-}$ and $^{\bullet}OH$ confirmed by 5,5-dimethylpyrroline-*N*-oxide (DMPO)-trapped electron paramagnetic resonance (EPR) spectra. The fingerprint of six peaks and the four peaks are characteristic for $O_2^{\bullet-}$ and $^{\bullet}OH$ adducts, respectively. (c, d) Preparation and application of a ROS-trapping gel film for visualizing ROS production in coastal soils. The fluorescence imaging fully displayed the hot spots of ROS generation within ~2.5 mm below the soil−water interface. (e) Oxygen profile in coastal soils. The penetration depth of oxygen at the soil−water interface is about ~2.5 mm upon a shift from high tide to low tide. (f−h) Time series of ROS production: $O_2^{\bullet-}$ and $^{\bullet}OH$ were the cumulative concentrations, and H_2O_2 was the real-time concentration.

minerals and organic matter, also termed as "geobattery")[15] in tidal ROS production. Moreover, we compared the tidal ROS production efficiency with those via a classical photochemical route. Our results highlight tidal hydrological processes as a ubiquitous but previously overlooked source of ROS, which provides new insights into biogeochemical processes and pollutant dynamics in coastal soils.

MATERIALS AND METHODS

Fabrication of a ROS-Trapping Gel Film. The ROS-trapping gel film was fabricated using a custom-made plastic binding plate. The mixture of agar gel prepared with phosphate-buffered saline (PBS) buffer (10 mM; pH 7.0) and 100 μM 2′,7′-dichlorodihydrofluorescein diacetate (H_2DCFDA, a fluorescent ROS probe)[23] was filled into the plate. After solidification for 2 h at 4 °C in the dark, the plate was covered with a poly(vinylidene fluoride) (PVDF) filter membrane (Whatman, 0.45 μm pore size). ROS production was semiquantitatively assessed by measuring the formation of a fluorescent product 2′,7′-dichlorofluorescein (DCF) through ROS-mediated oxidation of H_2DCFD.[23,24] The fluorescence of DCF was recorded by a confocal laser scanning microscope (Nikon Eclipse Ti2, Inc.) at an excitation wavelength of 488 nm and an emission wavelength of 525 nm. The application of the ROS-trapping gel film for ROS detection was validated using H_2O_2 as a representative ROS, where H_2O_2 exposure of films led to distinct green fluorescence formation and this fluorescence signal increased with increasing H_2O_2 concentrations (Figure S1). We further investigated the influence of PBS buffer on ROS measurement by comparing the fluorescence intensity assessed in PBS and borate buffer. The results showed that the buffer could affect ROS detection, yet to a minor extent (Figure S2). Because, in this study, we only applied the ROS-trapping gel film for assessing ROS spatial

https://doi.org/10.1021/acs.est.2c03142
Environ. Sci. Technol. 2022, 56, 11888−11896

distribution instead of quantitative analysis, the influence of buffer did not affect the ROS distribution result.

Lab-Simulated Tidal ROS Production. Fresh soils collected from the coastal wetland in the Yellow River Delta (37°42′N, 119°20′E) were placed into a custom-made polyethylene pipe (diameter = 10 cm), followed by addition of 2 L oxygen-free seawater (prepared using sea salts, salinity = 3.0%) and *Shewanella oneidensis* strain MR-1 (~3.0×10^8 cell/mL) (Section S1). Coastal soils were covered with a plastic film and incubated in the dark at room temperature for 21 days. Afterward, the overlying water was drained and soil ROS productions were qualitatively assessed by in situ electron paramagnetic resonance (EPR), quantitatively assessed with chemical probes, and visualized by the ROS-trapping gel film. To determine the rhythmic production of ROS, coastal soils were intermittently incubated at high tide (covered with 25 cm seawater) and low tide (covered with 1 cm seawater). The ROS productions were assessed with chemical probes.

ROS Detection. We applied three methods to qualitatively and quantitatively probe ROS productions in coastal soils with spatial and temporal resolutions.

Spatial Distribution of ROS by the Gel Film. The spatial distribution of ROS at the soil−water interface was detected using the as-prepared ROS-trapping gel film coupled with a confocal microscope (Nikon Eclipse Ti2, Inc.). The ROS-trapping gel film was perpendicularly inserted into the anoxic soil−water interface. After ROS capture, the ROS-trapping gel film was placed on a confocal microscope to visualize the spatial distribution of overall ROS, including $O_2^{\bullet-}$, H_2O_2, and $^{\bullet}OH$. The fluorescence of the H_2DCFDA reaction product with ROS was detected at an excitation of 488 nm and an emission of 525 nm. The overlying water in the control group was not drained to avoid air oxidation.

Qualification of ROS by In Situ Electron Paramagnetic Resonance (EPR). EPR analyses were applied for in situ and qualitative detection of ROS production. Next, 10 mL of 5,5-dimethylpyrroline-*N*-oxide (DMPO) solution (100 mM) was added to the reduced coastal soils for $^{\bullet}OH$ analysis.[25,26] Control samples were prepared under a N_2 atmosphere to prevent soil oxidation. For $O_2^{\bullet-}$ analysis, 5.0 g of reduced coastal soils was mixed with 10 mL of dimethyl sulfoxide (DMSO), followed by addition of 10 mL of DMPO (200 mM) prepared in DMSO as $O_2^{\bullet-}$ trap.[6] DMSO is widely applied as the solvent for EPR analyses of $O_2^{\bullet-}$ [27,28] because the $O_2^{\bullet-}$ adduct is more stabilized in polar aprotic solvents.[29] The samples were then analyzed using a Bruker-ESRA300 electron spin resonance spectrometer.

Temporal Production of ROS by Chemical Probes. Dipotassium terephthalate (TPA) was applied as a chemical probe to quantitatively detect $^{\bullet}OH$ production.[30] An excessive amount of TPA probe (1 mM) was added into the reduced coastal soils, and $^{\bullet}OH$ production was assessed by measuring the formation of hydroxyterephthalate (hTPA) through $^{\bullet}OH$-mediated hydroxylation of TPA. Adsorption control shows minor adsorption of hTPA (<10%) on soils (Figure S3). Thus, the TPA probe can be applied to measure $^{\bullet}OH$ in soils.[10,31] To ensure that the TPA probe was evenly distributed at the soil−water surface, we used a needle to gently stir the overlying TPA solution before sampling. At designed time points, aliquots (500 μL) were collected from the soil−water interface and immediately filtered through a 0.22 μm membrane for hTPA measurement. The fluorescence of hTPA was measured by an Agilent 1260 Infinity II high-performance liquid chromatograph (HPLC) equipped with a fluorescence detector (FLR, excitation wavelength = 250 nm, emission wavelength = 410 nm). The cumulative concentration of $^{\bullet}OH$ was determined with a hTPA formation yield of 0.35 upon the hydroxylation of TPA by reacting with $^{\bullet}OH$.[32] Ampliflu Red was used to probe the H_2O_2 generation by the formation of resorufin in the presence of horseradish peroxidase.[33] A 2,3-bis(2-methoxy-4-nitro-5-sulfophenyl)-2*H*-tetrazolium-5-carboxanilide (XTT) probe was used to measure the $O_2^{\bullet-}$ production.[34] $^{\bullet}OH$ and $O_2^{\bullet-}$ were the cumulative concentrations, and H_2O_2 was the real-time concentration. The detailed operating steps on the determination of H_2O_2 and $O_2^{\bullet-}$ are summarized in Section S2.

Field Investigations on Tidal ROS Production. ROS productions at six sampling sites were assessed along the coast of China. Site 1 (39°2′31″N, 117°48′33″E) was along the Bohai Sea; sites 2 (37°7′53″N, 122°27′10″E) and 3 (35°55′16″N, 120°7′58″E) were along the Yellow Sea; sites 4 (30°51′37″N, 121°54′57″E) and 5 (24°33′51″N, 118°3′44″E) were along the East China Sea; and site 6 (22°31′27″N, 113°57′43″E) was along the South China Sea. We designed an "enclosure experiment" via drilling two chambers using a poly(vinyl chloride) pipe without disturbing the soil−water interface at an intertidal zone (Figure S4). Fifty milliliters of potassium terephthalic acid probe solution (1 mM) was immediately injected, and the chamber was covered with aluminum foil to avoid photochemical ROS productions. Aliquots (900 μL) were collected from the supernatant at designed time points and immediately mixed with methanol (100 μL) to scavenge $^{\bullet}OH$ production in subsequent processes.[35] Samples were stored in a heat-insulated box filled with an ice chest and analyzed within 48 h.

Characterizations of Redox-Active Substances in Coastal Soils. Reactive iron in coastal soils was extracted with HCl and analyzed following the 1,10-phenanthroline method.[20,36] Reactive Fe(II) and total reactive Fe were determined by measuring the absorbance of ferrous and phenanthroline complexes before and after adding hydroxylamine hydrochloride as a Fe(III) reductant. Reactive Fe(III) was calculated as the difference between total reactive Fe and Fe(II). Acid volatile sulfide (AVS) represents reactive-reduced inorganic sulfur in coastal soils and was analyzed following a sequential extraction method.[37] Humic acid was isolated from coastal soils following the International Humic Substances Society (IHSS) procedure (Section S3).[38] EPR spectra of organic matter at high tide or low tide were measured in quartz glass tubes closed with plastic caps and parafilm (EMX 10/12, Bruker, Germany).[39] The chemical structure of organic matter extracted from coastal soils was analyzed using a solid-state ^{13}C nuclear magnetic resonance spectrometer (^{13}C NMR, Burker Avance III HD 400 WB) and a Fourier-transform infrared (FTIR) spectrometer (Nicolet iS10, Thermo).[6]

RESULTS AND DISCUSSION

Tide-Triggered ROS Production in Coastal Soils. We set out to detect tide-triggered ROS production in coastal soils with a spatial and temporal resolution under lab incubation. Coastal soils were first incubated with seawater at high tide, and then, the overlying seawater was drained at low tide to expose the reduced coastal soils to air. In situ EPR analysis indicated no ROS production at high tide. In comparison, tide receding resulted in distinctive formation of $O_2^{\bullet-}$ and $^{\bullet}OH$, as indicated by the fingerprint of six peaks and the four peaks that

https://doi.org/10.1021/acs.est.2c03142
Environ. Sci. Technol. 2022, 56, 11888−11896

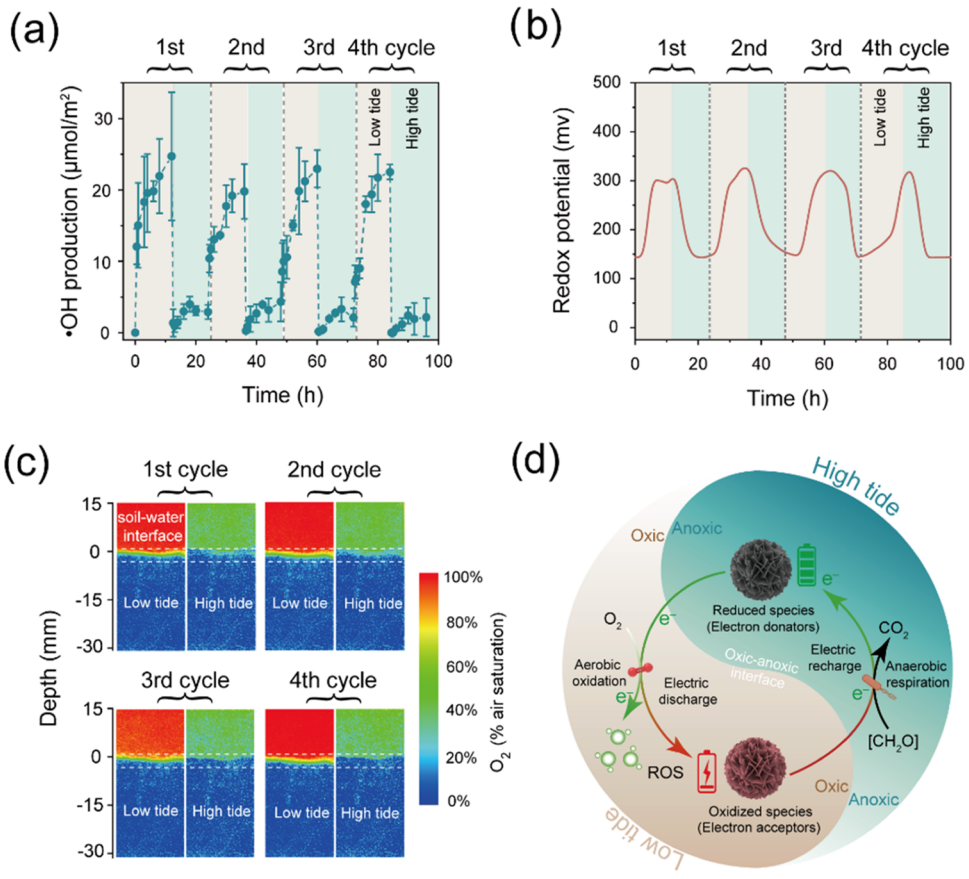

Figure 2. Rhythmic production of ROS and changes in geochemical conditions. (a) Rhythmic production of •OH. (b, c) Rhythmic changes in redox potential and oxygen content. (d) Schematic illustration of the tide-triggered rhythmic production of ROS.

are characteristic for both the $O_2^{\bullet-}$ and •OH adducts,[40] respectively (Figure 1b).

To visualize the spatial distribution of ROS in coastal soils, we developed a ROS-trapping gel film by immobilizing a ROS fluorescent probe in an agarose gel, which was perpendicularly placed in soils for in situ ROS probing (Figure 1c). ROS production in soils at low tide was confirmed by distinct fluorescence signals in the ROS-trapping gel film. The fluorescence imaging fully displayed the hot spots of ROS generation within ~2.5 mm below the soil−water interface (Figure 1d). The gradient ROS distribution resembled those of oxygen with a penetration depth of ~2.5 mm (Figure 1e), suggesting that the oxygen permeation at low tide is the direct drive for ROS production (Section S4). Accordingly, with inhibited oxygen permeation at high tide (Figure 1e), no ROS formation was observed (Figure 1d). We note that the classical photochemical production of ROS was temporally constrained to daytime and spatially constrained to the top 0.1−0.4 mm of the soils because of limited sunlight penetration depth.[6,7] Therefore, the tide-triggered dark pathway for ROS formation substantially broadens the spatial−temporal productions of ROS in coastal soils.

Further kinetic analysis showed rapid productions of $O_2^{\bullet-}$, H_2O_2, and •OH upon the shift from high tide to low tide (Figure 1f−h), suggesting the existence of electron-storing geobattery materials that can readily accumulate electrons at high tide and transfer electrons to infiltrated oxygen at low tide for ROS production. One-electron transfer from the reduced geobattery materials to molecular oxygen could lead to the rapid formation of $O_2^{\bullet-}$ (Figure 1f). Those $O_2^{\bullet-}$ radicals were metastable and transformed into H_2O_2 via dismutation and hydrolysis (Figure 1g),[31] which could undergo further reactions (e.g., Fenton's reaction, H_2O_2 + Fe(II) → •OH + Fe(III) + OH^-) to produce •OH (Figure 1h).[5] The Fenton reaction consumption of H_2O_2 with coastal soil-abundant iron minerals was confirmed by the drop in steady-state H_2O_2 concentration after ~8 h (Figure 1g). The electrons in geobattery materials were likely consumed after 5−10 h, as indicated by the obtained plateau of ROS production (Figure 1f−h). In comparison, minor production of ROS was observed in soils at high tide. Sterilized (inactivated) controls (treated with 1% $HgCl_2$) showed no significant change in •OH production (Figure S5), indicating that ROS production was mainly driven by abiotic processes.

Rhythmic Fluctuation of Tide-Triggered ROS Production. The stark contrast of ROS production under high tide and low tide conditions begs an important question: Is the tide-triggered ROS production rhythmic and sustainable? To address this question, we chose the •OH radical, a potent ROS species in the environment[41] and a key player for element cycles[42] as a representative ROS, and monitored its production over four tidal cycles under lab incubations (Figures 2 and S6). Notably, •OH is produced through reactions of $O_2^{\bullet-}$ and H_2O_2, and productions of •OH also indicate the formations of H_2O_2 and $O_2^{\bullet-}$.[5] The soil •OH production exhibited a distinct rhythmic fluctuation, with the production as high as 25 μmol/m^2 at low tide and <5 μmol/m^2 at high tide (Figure 2a). The small •OH production at high tide is likely caused by the reaction of residual oxygen with a reduced geobattery material (Figure 2b). In addition, the •OH production was sustainable

https://doi.org/10.1021/acs.est.2c03142
Environ. Sci. Technol. 2022, 56, 11888−11896

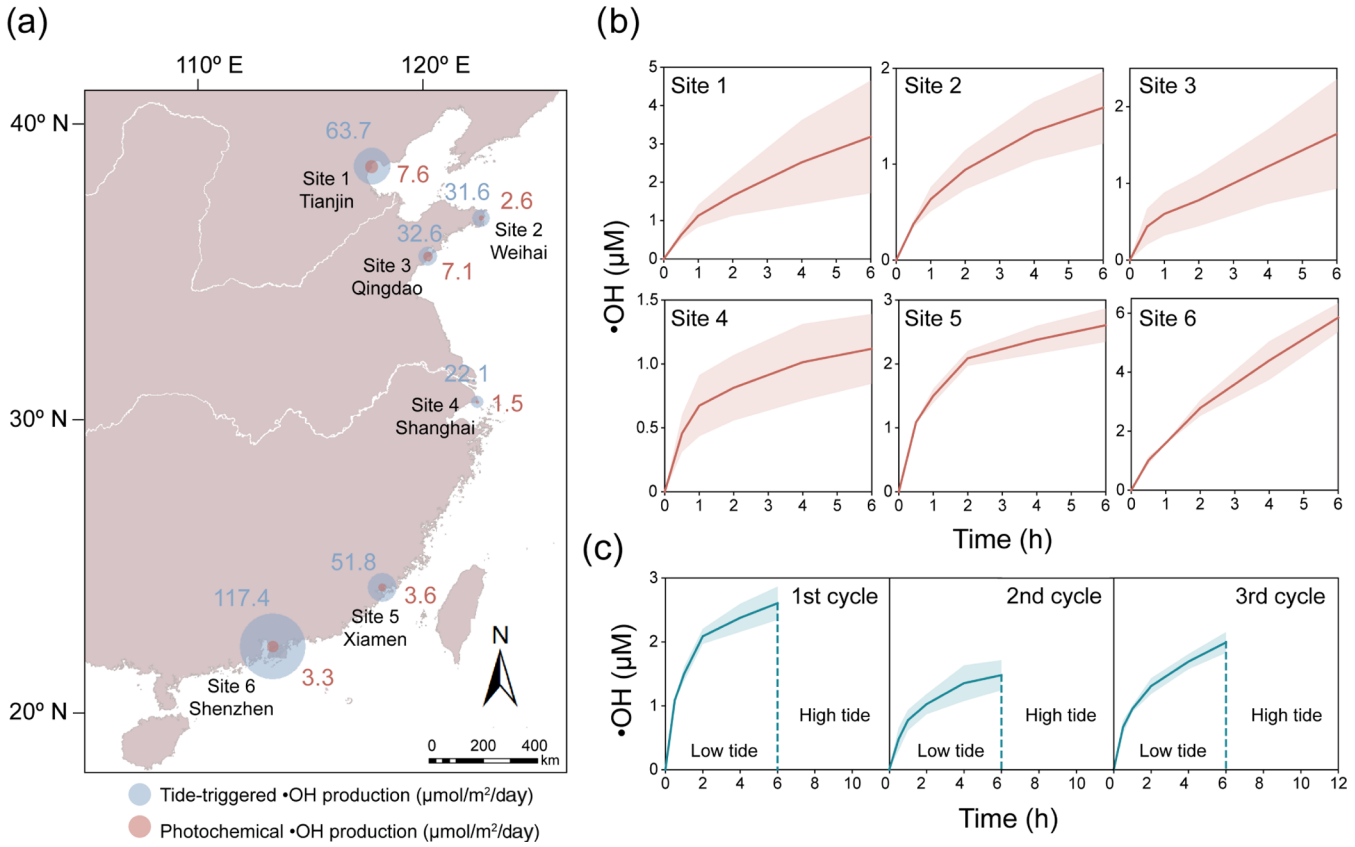

Figure 3. In situ characterization of tide-triggered ROS production along the coast of China. (a) Field site map showing area-normalized •OH production. The circle size represents the •OH production flux. (b) Time series of •OH production at sites 1−6. (c) Rhythmic production of •OH (showing site 5 as an example).

with no obvious decline in the production amount over several tidal cycles, demonstrating that soil electron-storing geobattery materials in coastal soils are regenerable. Such rechargeability may be affected by degradation of redox-active moieties (e.g., phenolic moieties),[39] formation of phenolic/quinone moieties,[43] and activation of Fe minerals.[44] Notably, the charging degree of the geobattery material is affected by multiple factors such as microbial activity and charging time, where the 12-h charging period applied based on natural conditions is unlikely to achieve full charging. Compared to redox-stable ecosystems (e.g, lake sediments) and ecosystems with redox fluctuations yet at low frequency (e.g., 1−3 cycles per year in rice paddy), the coastal soils with tide-induced frequent redox fluctuations (i.e., 1−2 cycles per day) represent unique sites for the sustainable and rhythmic generation of ROS.

The oscillations on the redox potential and dissolved oxygen concentration followed the same pattern as the •OH production, confirming the alternating oxic−anoxic conditions as the main geochemical drive for ROS production (Figure 2b,c). A shift from low tide to high tide condition leads to a decrease of redox potential from 300 to 150 mV (Figure 2b), coupled with dissolved oxygen content decreasing from 100% air saturation to <20% air saturation in coastal soils (Figure 2c). Notably, ROS productions in coastal soils and inland unconfined aquifers show an opposite dependence on water table fluctuations. For inland aquifers, rising water brought dissolved oxygen to react with reduced species in anoxic soils for ROS production in the rainy season.[11] In stark contrast, in coastal soils, the rising seawater isolates surface soils from air, leading to the decline in oxygen content. We speculated that at high tide with deficient oxygen, microbe anaerobic respiration could release electrons to the electron-storing materials,[45,46] inducing soil geobattery "charging". Upon shifting to low tide, atmospheric oxygen penetrated into the soil, leading to the increase of soil redox potential. In the meantime, the "discharge" of soil geobattery materials to oxygen resulted in the formation of ROS in coastal soils (Figure 2d).

In Situ Characterization of Tide-Triggered ROS Production along the Coast of China. We then in situ tested whether the tidal fluctuations could ubiquitously trigger ROS production in the natural field under varying biogeochemical and climatic conditions (Table S1 and Figure S7). Field assessments of ROS production were conducted at six sampling sites along the coast of China (Figure 3a). The in situ analyses confirmed •OH production in coastal soils at all investigated sites. ROS production at low tide followed the same pattern as the lab simulations, with cumulative •OH productions ranging from 1.1 to 5.9 μM after one complete semidiurnal tide (Figure 3b). Accordingly, the daily flux of •OH production at six sampling sites was calculated to be 22.1−117.4 μmol/m^2/day (Figure 3a). Moreover, ROS production in coastal soils by natural tides also exhibited sustainable and rhythmic patterns, as indicated by the cyclical •OH production over consecutive tides (Figures 3c and S8).

To compare the tide-triggered •OH productions with those via classical photochemical routes, we further assessed the photochemical production of ROS on the soil surface under 1 sun irradiation condition (100 mW/cm^2, AM 1.5G; Figure S9) under lab incubation. The cumulative productions of •OH via

https://doi.org/10.1021/acs.est.2c03142
Environ. Sci. Technol. 2022, 56, 11888−11896

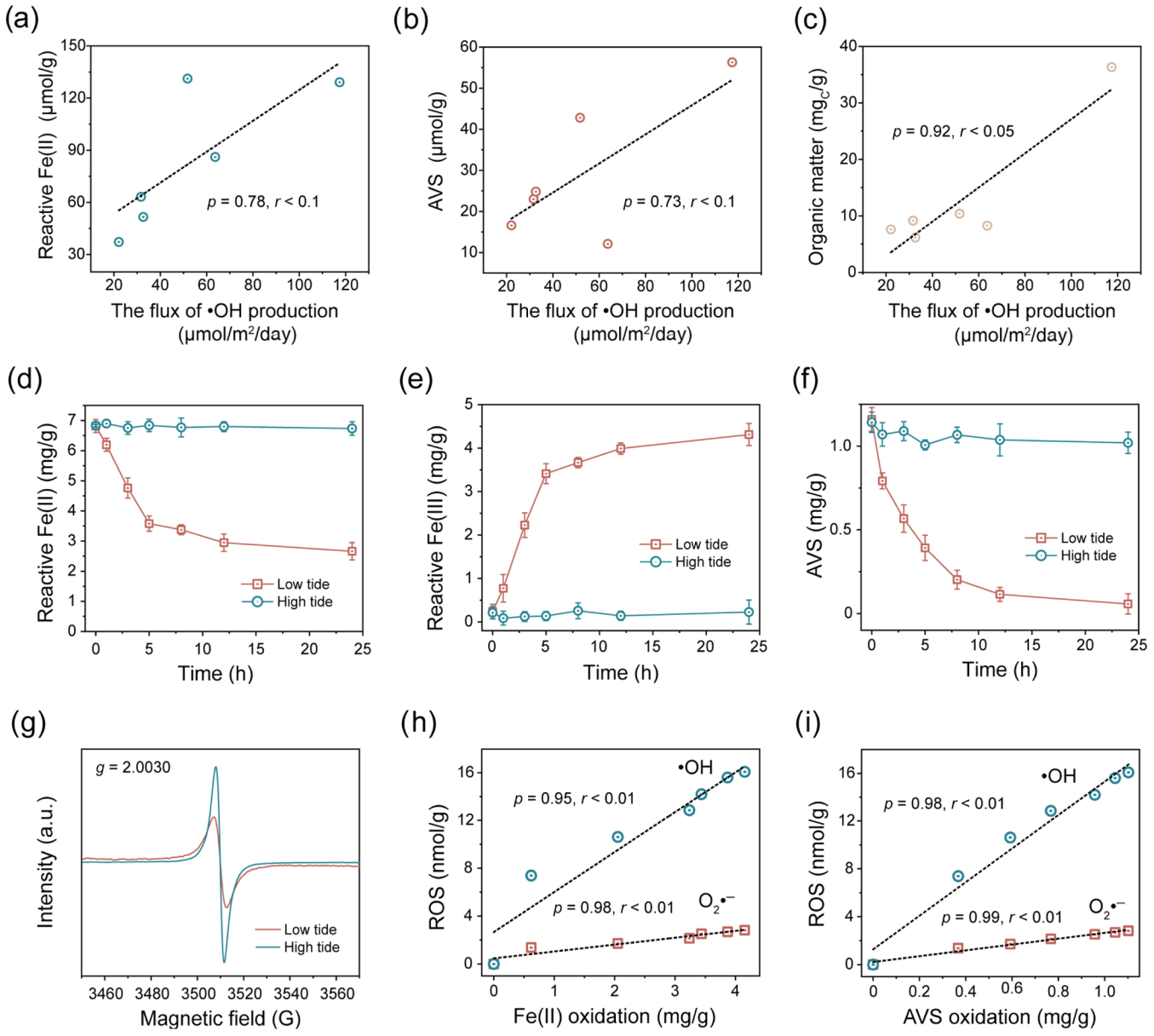

Figure 4. Tidal production of ROS regulated by soil redox-active components. Relationship between •OH production and abundance of redox-active geobattery materials in field coastal soils, including (a) reactive Fe(II), (b) acid volatile sulfide (AVS), (c) organic matter shown as total organic carbon (TOC). Coastal soils collected from the field were incubated under anoxic conditions for 21 days before the experiment. (d, e) Reactive ferrous iron (Fe II) and ferric iron (Fe III) in coastal soils at high tide and low tide. (f) Acid volatile sulfide (AVS) in coastal soils at high tide and low tide. (g) Electron paramagnetic resonance spectra of humic acid extracted from coastal soils. Correlation of ROS production with the oxidation of (h) Fe(II) and (i) AVS.

photochemical routes ranged from 0.08 to 0.38 μM over the course of a semidiurnal tide. The daily flux of •OH production at six sampling sites was calculated to be 1.5−7.6 μmol/m^2/day (Figure 3a). The tide-triggered •OH production was 5- to 36-fold more efficient than those via classical photochemical routes over the course of a semidiurnal tide. We note that the tidal ROS production efficiency is dependent on hydrological conditions, microbial activity, and soil properties. In the meantime, the incident sunlight intensity may profoundly vary depending on numerous factors (e.g., cloud cover, atmospheric gases, and particles), which can affect photochemical ROS productions.[30] Therefore, the relative importance of tidal and photochemical ROS productions in coastal biogeochemical processes may vary depending on environmental conditions.

Tidal ROS Regulated by Soil Redox-Active Components. Physicochemical property analyses on coastal soils showed that the •OH productions were positively related to the abundance of soil electron-storing geobattery materials, such as reactive Fe(II) and acid volatile sulfide (Figure 4a−c). For instance, clay soils contain more electron-storing materials than sandy soils. Accordingly, higher •OH productions at site 6 (clay = 9%, sand = 30%) were observed than those at site 4 (clay = 2%, sand = 60%) (Figure S10 and Table S1). To illustrate the role of interactions between tidal hydrology and soil biogeochemistry on ROS production, we analyzed the dynamics of redox-active substances under lab incubation. A shift from high tide to low tide condition leads to a decrease of reactive Fe(II) from 7 to 2.5 mg/g (Figure 4d), coupled with

https://doi.org/10.1021/acs.est.2c03142
Environ. Sci. Technol. 2022, 56, 11888−11896

an increase of reactive Fe(III) from 0.5 to 4.5 mg/g (Figure 4e). Similarly, AVS decreased from 1.2 mg/g at high tide to 0.1 mg/g at low tide (Figure 4f), indicating the oxidation of labile metal sulfides to sulfate and metal oxides.[47] In stark contrast, control samples incubated under continuous high tide showed minor changes in Fe(II), Fe(III), and AVS contents. In addition, EPR spectra of organic matter extracted from coastal soils indicate the existence of semiquinone radicals (Figure 4g).[39] The semiquinone intensity decreased upon shifting from high tide to low tide. The ^{13}C NMR and FTIR spectra further confirmed the existence of redox-active components such as quinone and phenolic moieties in coastal organic matter (Figure S11).[48−51] The above results support our hypothesis that reactive Fe and S minerals and organic carbon abundant in coastal soils can serve as geobatteries for electron storage, and their charging states were regulated by tidal hydrological conditions. More importantly, the tide-induced turnovers on the redox states of soil electron-storing geobattery materials were consistent with the tidal ROS production (Figure 4h,i), demonstrating the key roles of soil redox-active components in regulating tidal ROS productions.

■ ENVIRONMENTAL IMPLICATIONS

Our study constructed a biogeochemical−hydrological framework for ROS production in surface coastal soils. The tidal fluctuations triggered redox oscillations of soil electron-storing geobattery materials, leading to widespread and rhythmic productions of ROS. Such a dark redox pathway for ROS formation, as proven to be more efficient than ROS production via classical photochemical routes, substantially broadens the spatial−temporal productions of ROS in coastal soils.

The sustainable production of ROS in coastal soils at a high frequency could lead to profound impacts on biogeochemical processes such as organic carbon decomposition. Carbon sequestration in coastal soils has been suggested as a key natural climate solution,[52] yet improved predictions of carbon storage demand better integration of key biogeochemical mechanisms controlling organic carbon decomposition. Here, due to the rapid reaction of $^{\bullet}OH$ with organic carbon (10^8 M^{-1} s^{-1}),[53] direct oxidation of organic matter by $^{\bullet}OH$ alone could mineralize organic carbon to CO_2 at a rate of 22.1−117.4 $\mu mol/m^2/day$, with yields of 0.30 mol CO_2 per mol $^{\bullet}OH$.[10] Moreover, $^{\bullet}OH$ and other ROS species could accelerate coastal soil carbon mineralization by degrading the recalcitrant carbon (e.g., lignin) to more microbially available forms such as low-molecular-weight fatty acids.[54] Furthermore, the oxidation of soil organic carbon will enhance the bioavailability of buried nutrients (e.g., phosphate)[51,55] and promote the release of trace metals (e.g., mercury).[56] In addition, given that coastal soils are among the major natural sinks for environmental pollutants (e.g., crude oil, pesticides, and microplastics), tidal ROS could play a key role in the natural purification of polluted soils.

■ ASSOCIATED CONTENT

Supporting Information

The Supporting Information is available free of charge at https://pubs.acs.org/doi/10.1021/acs.est.2c03142.

Supporting figures, tables, detailed experimental methods and the results of additional experiments described in the manuscript (PDF)

■ AUTHOR INFORMATION

Corresponding Author

Chiheng Chu − *Faculty of Agriculture, Life, and Environmental Sciences, Zhejiang University, Hangzhou 310058, China;* orcid.org/0000-0001-9493-9120; Email: chuchiheng@zju.edu.cn

Authors

Guoqiang Zhao − *Faculty of Agriculture, Life, and Environmental Sciences, Zhejiang University, Hangzhou 310058, China;* orcid.org/0000-0002-6632-6412

Binbin Wu − *Faculty of Agriculture, Life, and Environmental Sciences, Zhejiang University, Hangzhou 310058, China*

Xiaoshan Zheng − *Faculty of Agriculture, Life, and Environmental Sciences, Zhejiang University, Hangzhou 310058, China*

Baoliang Chen − *Faculty of Agriculture, Life, and Environmental Sciences, Zhejiang University, Hangzhou 310058, China;* orcid.org/0000-0001-8196-081X

Andreas Kappler − *Geomicrobiology, Center for Applied Geosciences, University of Tübingen, 72074 Tübingen, Germany; Cluster of Excellence: EXC 2124: Controlling Microbes to Fight Infection, 72074 Tübingen, Germany;* orcid.org/0000-0002-3558-9500

Complete contact information is available at: https://pubs.acs.org/10.1021/acs.est.2c03142

Notes

The authors declare no competing financial interest.

Data that support the findings of this study are available from the corresponding authors upon reasonable request.

■ ACKNOWLEDGMENTS

This work was supported by the National Natural Science Foundation of China (NSFC, Nos. 22136004, 42107392, 22006129) and the project funded by China Postdoctoral Science Foundation (No. 2021M692774). A.K. acknowledges infrastructural support by the DFG under Germany's Excellence Strategy, cluster of Excellence EXC2124, project ID 390838134.

■ REFERENCES

(1) Shaw, T. J.; Luther, G. W.; Rosas, R.; Oldham, V. E.; Coffey, N. R.; Ferry, J. L.; Dias, D. M. C.; Yücel, M.; Thibault de Chanvalon, A. Fe-catalyzed sulfide oxidation in hydrothermal plumes is a source of reactive oxygen species to the ocean. *Proc. Natl. Acad. Sci. U.S.A.* **2021**, *118*, No. e2026654118.

(2) Zhang, P.; Yuan, S. Production of hydroxyl radicals from abiotic oxidation of pyrite by oxygen under circumneutral conditions in the presence of low-molecular-weight organic acids. *Geochim. Cosmochim. Acta* **2017**, *218*, 153−166.

(3) Kleber, M.; Bourg, I. C.; Coward, E. K.; Hansel, C. M.; Myneni, S. C. B.; Nunan, N. Dynamic interactions at the mineral−organic matter interface. *Nat. Rev. Earth Environ.* **2021**, *2*, 402−421.

(4) Yuan, S.; Liu, X.; Liao, W.; Zhang, P.; Wang, X.; Tong, M. Mechanisms of electron transfer from structrual Fe(II) in reduced nontronite to oxygen for production of hydroxyl radicals. *Geochim. Cosmochim. Acta* **2018**, *223*, 422−436.

(5) Diaz, J. M.; Hansel, C. M.; Voelker, B. M.; Mendes, C. M.; Andeer, P. F.; Zhang, T. Widespread production of extracellular superoxide by heterotrophic bacteria. *Science* **2013**, *340*, 1223−1226.

(6) Huang, Y.-N.; Qian, T.-T.; Dang, F.; Yin, Y.-G.; Li, M.; Zhou, D.-M. Significant contribution of metastable particulate organic

matter to natural formation of silver nanoparticles in soils. *Nat. Commun.* **2019**, *10*, No. 3775.
(7) Hebert, V. R.; Miller, G. C. Depth dependence of direct and indirect photolysis on soil surfaces. *J. Agric. Food Chem.* **1990**, *38*, 913−918.
(8) Sutherland, K. M.; Wankel, S. D.; Hansel, C. M. Dark biological superoxide production as a significant flux and sink of marine dissolved oxygen. *Proc. Natl Acad. Sci. U.S.A.* **2020**, *117*, 3433−3439.
(9) Zhang, T.; Hansel, C. M.; Voelker, B. M.; Lamborg, C. H. Extensive dark biological production of reactive oxygen species in brackish and freshwater ponds. *Environ. Sci. Technol.* **2016**, *50*, 2983−2993.
(10) Page, S. E.; Kling, G. W.; Sander, M.; Harrold, K. H.; Logan, J. R.; McNeill, K.; Cory, R. M. Dark formation of hydroxyl radical in arctic soil and surface waters. *Environ. Sci. Technol.* **2013**, *47*, 12860−12867.
(11) Zhang, N.; Bu, X.; Li, Y.; Zhang, Y.; Yuan, S.; Wen, Z.; Tong, M.; Lin, L. Water table fluctuations regulate hydrogen peroxide production and distribution in unconfined aquifers. *Environ. Sci. Technol.* **2020**, *54*, 4942−4951.
(12) Yuan, X.; Nico, P. S.; Huang, X.; Liu, T.; Ulrich, C.; Williams, K. H.; Davis, J. A. Production of hydrogen peroxide in groundwater at Rifle, Colorado. *Environ. Sci. Technol.* **2017**, *51*, 7881−7891.
(13) Murphy, S. A.; Solomon, B. M.; Meng, S.; Copeland, J. M.; Shaw, T. J.; Ferry, J. L. Geochemical production of reactive oxygen species from biogeochemically reduced Fe. *Environ. Sci. Technol.* **2014**, *48*, 3815−3821.
(14) Du, H.; Cao, Y.; Li, Z.; Li, L.; Xu, H. Formation and mechanisms of hydroxyl radicals during the oxygenation of sediments in Lake Poyang, China. *Water Res.* **2021**, *202*, No. 117442.
(15) Peiffer, S.; Kappler, A.; Haderlein, S. B.; Schmidt, C.; Byrne, J. M.; Kleindienst, S.; Vogt, C.; Richnow, H. H.; Obst, M.; Angenent, L. T.; Bryce, C.; McCammon, C.; Planer-Friedrich, B. A biogeochemical-hydrological framework for the role of redox-active compounds in aquatic systems. *Nat. Geosci.* **2021**, *14*, 264−272.
(16) Wang, X.; Xiao, X.; Xu, X.; Zou, Z.; Chen, B.; Qin, Y.; Zhang, X.; Dong, J.; Liu, D.; Pan, L.; Li, B. Rebound in China's coastal wetlands following conservation and restoration. *Nat. Sustainability* **2021**, *4*, 1076−1083.
(17) Bertram, C.; Quaas, M.; Reusch, T. B. H.; Vafeidis, A. T.; Wolff, C.; Rickels, W. The blue carbon wealth of nations. *Nat. Clim. Change* **2021**, *11*, 704−709.
(18) Mascarelli, A. Deepwater horizon: after the oil. *Nature* **2010**, *467*, 22−24.
(19) Xie, Z.; Wang, P.; Wang, X.; Castro-Jiménez, J.; Kallenborn, R.; Liao, C.; Mi, W.; Lohmann, R.; Vila-Costa, M.; Dachs, J. Organophosphate ester pollution in the oceans. *Nat. Rev. Earth Environ.* **2022**, *3*, 309.
(20) Byrne, J. M.; Klueglein, N.; Pearce, C.; Rosso, K. M.; Appel, E.; Kappler, A. Redox cycling of Fe(II) and Fe(III) in magnetite by Fe-metabolizing bacteria. *Science* **2015**, *347*, 1473−1476.
(21) Kessler, A. J.; Chen, Y.-J.; Waite, D. W.; Hutchinson, T.; Koh, S.; Popa, M. E.; Beardall, J.; Hugenholtz, P.; Cook, P. L. M.; Greening, C. Bacterial fermentation and respiration processes are uncoupled in anoxic permeable sediments. *Nat. Microbiol.* **2019**, *4*, 1014−1023.
(22) Kappler, A.; Bryce, C.; Mansor, M.; Lueder, U.; Byrne, J. M.; Swanner, E. D. An evolving view on biogeochemical cycling of iron. *Nat. Rev. Microbiol.* **2021**, *19*, 360−374.
(23) Mangano, S.; Denita-Juarez, S. P.; Choi, H.-S.; Marzol, E.; Hwang, Y.; Ranocha, P.; Velasquez, S. M.; Borassi, C.; Barberini, M. L.; Aptekmann, A. A.; Muschietti, J. P.; Nadra, A. D.; Dunand, C.; Cho, H.-T.; Estevez, J. M. Molecular link between auxin and ROS-mediated polar growth. *Proc. Natl Acad. Sci. U.S.A.* **2017**, *114*, 5289−5294.
(24) Ma, W.; Pang, Z.; Huang, X.; Xu, J.; Pandey, S. S.; Li, J.; Achor, D. S.; Vasconcelos, F. N. C.; Hendrich, C.; Huang, Y.; Wang, W.; Lee, D.; Stanton, D.; Wang, N. Citrus Huanglongbing is a pathogen-triggered immune disease that can be mitigated with antioxidants and gibberellin. *Nat. Commun.* **2022**, *13*, No. 529.
(25) Huang, H.; Ji, X.-B.; Cheng, L.-Y.; Zhao, F.-J.; Wang, P. Free radicals produced from the oxidation of ferrous sulfides promote the remobilization of cadmium in paddy soils during drainage. *Environ. Sci. Technol.* **2021**, *55*, 9845−9853.
(26) Zhao, Y.; Xiang, W.; Huang, C.; Liu, Y.; Tan, Y. Production of hydroxyl radicals following water-level drawdown in peatlands: A new induction mechanism for enhancing laccase activity in carbon cycling. *Soil Biol. Biochem.* **2021**, *156*, No. 108241.
(27) Li, Y.; Zhao, J.; Shang, E.; Xia, X.; Niu, J.; Crittenden, J. Effects of chloride ions on dissolution, ROS generation, and toxicity of silver nanoparticles under UV irradiation. *Environ. Sci. Technol.* **2018**, *52*, 4842−4849.
(28) Li, Y.; Niu, J.; Shang, E.; Crittenden, J. C. Synergistic photogeneration of reactive oxygen species by dissolved organic matter and C60 in aqueous phase. *Environ. Sci. Technol.* **2015**, *49*, 965−973.
(29) Villamena, F. A.; Xia, S.; Merle, J. K.; Lauricella, R.; Tuccio, B.; Hadad, C. M.; Zweier, J. L. Reactivity of superoxide radical anion with cyclic nitrones: Role of intramolecular H-bond and electrostatic effects. *J. Am. Chem. Soc.* **2007**, *129*, 8177−8191.
(30) Wu, B.; Liu, T.; Wang, Y.; Zhao, G.; Chen, B.; Chu, C. High sample throughput LED reactor for facile characterization of the quantum yield spectrum of photochemically produced reactive intermediates. *Environ. Sci. Technol.* **2021**, *55*, 16204−16214.
(31) Georgiou, C. D.; Sun, H. J.; McKay, C. P.; Grintzalis, K.; Papapostolou, I.; Zisimopoulos, D.; Panagiotidis, K.; Zhang, G.; Koutsopoulou, E.; Christidis, G. E.; Margiolaki, I. Evidence for photochemical production of reactive oxygen species in desert soils. *Nat. Commun.* **2015**, *6*, No. 7100.
(32) Chu, C.; Erickson, P. R.; Lundeen, R. A.; Stamatelatos, D.; Alaimo, P. J.; Latch, D. E.; McNeill, K. Photochemical and nonphotochemical transformations of cysteine with dissolved organic matter. *Environ. Sci. Technol.* **2016**, *50*, 6363−6373.
(33) Chu, C.; Zhu, Q.; Pan, Z.; Gupta, S.; Huang, D.; Du, Y.; Weon, S.; Wu, Y.; Muhich, C.; Stavitski, E.; Domen, K.; Kim, J.-H. Spatially separating redox centers on 2D carbon nitride with cobalt single atom for photocatalytic H_2O_2 production. *Proc. Natl Acad. Sci. U.S.A.* **2020**, *117*, 6376−6382.
(34) Fu, H.; Liu, H.; Mao, J.; Chu, W.; Li, Q.; Alvarez, P. J. J.; Qu, X.; Zhu, D. Photochemistry of dissolved black carbon released from biochar: reactive oxygen species generation and phototransformation. *Environ. Sci. Technol.* **2016**, *50*, 1218−1226.
(35) Chen, N.; Fu, Q.; Wu, T.; Cui, P.; Fang, G.; Liu, C.; Chen, C.; Liu, G.; Wang, W.; Wang, D.; Wang, P.; Zhou, D. Active iron phases regulate the abiotic transformation of organic carbon during redox fluctuation cycles of paddy soil. *Environ. Sci. Technol.* **2021**, *55*, 14281−14293.
(36) Wallmann, K.; Hennies, K.; Konig, I.; Petersen, W.; Knauth, H. D. New procedure for determining reactive Fe(III) and Fe(II) minerals in sediments. *Limnol. Oceanogr.* **1993**, *38*, 1803−1812.
(37) Hsieh, Y. P.; Shieh, Y. N. Analysis of reduced inorganic sulfur by diffusion methods: improved apparatus and evaluation for sulfur isotopic studies. *Chem. Geol.* **1997**, *137*, 255−261.
(38) Wen, B.; Zhang, J.; Zhang, S.; Shan, X.; Khan, S.; Xing, B. Phenanthrene sorption to soil humic acid and different humin fractions. *Environ. Sci. Technol.* **2007**, *41*, 3165−3171.
(39) Roden, E. E.; Kappler, A.; Bauer, I.; Jiang, J.; Paul, A.; Stoesser, R.; Konishi, H.; Xu, H. Extracellular electron transfer through microbial reduction of solid-phase humic substances. *Nat. Geosci.* **2010**, *3*, 417−421.
(40) Bonke, S. A.; Risse, T.; Schnegg, A.; Brückner, A. In situ electron paramagnetic resonance spectroscopy for catalysis. *Nat. Rev. Methods Primers* **2021**, *1*, No. 33.
(41) Tong, M.; Yuan, S.; Ma, S.; Jin, M.; Liu, D.; Cheng, D.; Liu, X.; Gan, Y.; Wang, Y. Production of abundant hydroxyl radicals from oxygenation of subsurface sediments. *Environ. Sci. Technol.* **2016**, *50*, 214−221.

https://doi.org/10.1021/acs.est.2c03142
Environ. Sci. Technol. 2022, 56, 11888−11896

(42) Gligorovski, S.; Strekowski, R.; Barbati, S.; Vione, D. Environmental Implications of Hydroxyl Radicals ($^{\bullet}$OH). *Chem. Rev.* **2015**, *115*, 13051−13092.
(43) Yang, P.; Jiang, T.; Cong, Z.; Liu, G.; Guo, Y.; Liu, Y.; Shi, J.; Hu, L.; Yin, Y.; Cai, Y.; Jiang, G. Loss and increase of the electron exchange capacity of natural organic matter during its reduction and reoxidation: The role of quinone and nonquinone moieties. *Environ. Sci. Technol.* **2022**, *56*, 6744−6753.
(44) Ginn, B.; Meile, C.; Wilmoth, J.; Tang, Y.; Thompson, A. Rapid iron reduction rates are stimulated by high-amplitude redox fluctuations in a tropical forest soil. *Environ. Sci. Technol.* **2017**, *51*, 3250−3259.
(45) Han, R.; Lv, J.; Huang, Z.; Zhang, S.; Zhang, S. Pathway for the Production of Hydroxyl Radicals during the Microbially Mediated Redox Transformation of Iron (Oxyhydr)oxides. *Environ. Sci. Technol.* **2020**, *54*, 902−910.
(46) Klüpfel, L.; Piepenbrock, A.; Kappler, A.; Sander, M. Humic substances as fully regenerable electron acceptors in recurrently anoxic environments. *Nat. Geosci.* **2014**, *7*, 195−200.
(47) Zhao, G.; Sheng, Y.; Jiang, M.; Yin, X. Redox-dependent phosphorus burial and regeneration in an offshore sulfidic sediment core in North Yellow Sea, China. *Mar. Pollut. Bull.* **2019**, *149*, No. 110582.
(48) Aeschbacher, M.; Graf, C.; Schwarzenbach, R. P.; Sander, M. Antioxidant Properties of Humic Substances. *Environ. Sci. Technol.* **2012**, *46*, 4916−4925.
(49) Li, C.; Zhang, B.; Ertunc, T.; Schaeffer, A.; Ji, R. Birnessite-Induced Binding of Phenolic Monomers to Soil Humic Substances and Nature of the Bound Residues. *Environ. Sci. Technol.* **2012**, *46*, 8843−8850.
(50) Wang, X.; Guo, X.; Yang, Y.; Tao, S.; Xing, B. Sorption Mechanisms of Phenanthrene, Lindane, and Atrazine with Various Humic Acid Fractions from a Single Soil Sample. *Environ. Sci. Technol.* **2011**, *45*, 2124−2130.
(51) Zhao, G.; Sheng, Y.; Li, C.; Liu, Q.; Hu, N. Restraint of enzymolysis and photolysis of organic phosphorus and pyrophosphate using synthetic zeolite with humic acid and lanthanum. *Chem. Eng. J.* **2020**, *386*, No. 123791.
(52) Sala, E.; Mayorga, J.; Bradley, D.; Cabral, R. B.; Atwood, T. B.; Auber, A.; Cheung, W.; Costello, C.; Ferretti, F.; Friedlander, A. M.; Gaines, S. D.; Garilao, C.; Goodell, W.; Halpern, B. S.; Hinson, A.; Kaschner, K.; Kesner-Reyes, K.; Leprieur, F.; McGowan, J.; Morgan, L. E.; Mouillot, D.; Palacios-Abrantes, J.; Possingham, H. P.; Rechberger, K. D.; Worm, B.; Lubchenco, J. Protecting the global ocean for biodiversity, food and climate. *Nature* **2021**, *592*, 397−402.
(53) Westerhoff, P.; Mezyk, S. P.; Cooper, W. J.; Minakata, D. Electron pulse radiolysis determination of hydroxyl radical rate constants with Suwannee River fulvic acid and other dissolved organic matter isolates. *Environ. Sci. Technol.* **2007**, *41*, 4640−4646.
(54) Patzner, M. S.; Mueller, C. W.; Malusova, M.; Baur, M.; Nikeleit, V.; Scholten, T.; Hoeschen, C.; Byrne, J. M.; Borch, T.; Kappler, A.; Bryce, C. Iron mineral dissolution releases iron and associated organic carbon during permafrost thaw. *Nat. Commun.* **2020**, *11*, No. 6329.
(55) Duhamel, S.; Diaz, J. M.; Adams, J. C.; Djaoudi, K.; Steck, V.; Waggoner, E. M. Phosphorus as an integral component of global marine biogeochemistry. *Nat. Geosci.* **2021**, *14*, 359−368.
(56) Tian, L.; Guan, W.; Ji, Y.; He, X.; Chen, W.; Alvarez, P. J. J.; Zhang, T. Microbial methylation potential of mercury sulfide particles dictated by surface structure. *Nat. Geosci.* **2021**, *14*, 409−416.

https://doi.org/10.1021/acs.est.2c03142
Environ. Sci. Technol. 2022, 56, 11888−11896